Supplementary material:
Holey sheets:Double-Threshold Rupture of Draining Liquid Films

Ayush K. Dixit,[1, *] Chunheng Zhao,[2, †] Stéphane Zaleski,[3, 4, ‡] Detlef Lohse,[1, 5, §] and Vatsal Sanjay[6, 1, ¶]

[1]*Physics of Fluids Department, Max Planck Center Twente for Complex Fluid Dynamics,*
and J. M. Burgers Center for Fluid Dynamics, University of Twente, P.O. Box 217, 7500AE Enschede, Netherlands
[2]*Department of Mechanical Engineering, City College of New York, New York, New York 10031, USA*
[3]*Sorbonne Université and CNRS, UMR 7190, Institut Jean Le Rond ∂'Alembert, 75005 Paris, France*
[4]*Institut Universitaire de France, UMR 7190, Institut Jean Le Rond ∂'Alembert, 75005 Paris, France*
[5]*Max Planck Institute for Dynamics and Self-Organisation, Am Fassberg 17, 37077 Göttingen, Germany*
[6]*CoMPhy Lab, Department of Physics, Durham University,*
Science Laboratories, South Road, Durham DH1 3LE, United Kingdom
(Dated: September 21, 2025)

CONTENTS

I. GOVERNING EQUATIONS

The governing dynamical equations have been solved using the free software Basilisk C [1, 2]. For all the quantities, length scales are normalized using the initial bubble radius, resulting in $\mathcal{L} = \tilde{\mathcal{L}} R_0$ as characteristic length, while the time is normalized using the inertiocapillary timescale $\tau_\gamma = \sqrt{\rho_s R_0{}^3/\gamma}$ giving $t = \tilde{t}\tau_\gamma$. These normalizations leads to an inertiocapillary velocity scale $u_\gamma = \sqrt{\gamma/\rho_s R_0}$ for the velocity field $\boldsymbol{u} = \tilde{\boldsymbol{u}} u_\gamma$. Lastly, stresses are normalized using the Laplace pressure scale, $\boldsymbol{\sigma} = \tilde{\boldsymbol{\sigma}} \sigma_\gamma$, where $\sigma_\gamma = \gamma/R_0$. The governing mass and momentum conservation equations for the liquid phase in dimensionless form read

$$\boldsymbol{\nabla} \cdot \boldsymbol{u} = 0 \, \text{and} \tag{1}$$

$$\frac{\partial \boldsymbol{u}}{\partial t} + \boldsymbol{\nabla} \cdot (\boldsymbol{u}\boldsymbol{u}) = -\boldsymbol{\nabla} p + 2 \, Oh \boldsymbol{\nabla} \cdot \boldsymbol{\mathcal{D}}, \tag{2}$$

where $\boldsymbol{\mathcal{D}} = \left(\boldsymbol{\nabla} \boldsymbol{u} + (\boldsymbol{\nabla} \boldsymbol{u})^T \right)/2$ represents the symmetric part of the velocity gradient tensor–equal to half of the rate-of-strain tensor, and p is the pressure field.

———

* a.k.dixit@utwente.nl
† czhao000@citymail.cuny.edu
‡ stephane.zaleski@sorbonne-universite.fr
§ d.lohse@utwente.nl
¶ vatsali.sanjay@comphy-lab.org

II. NUMERICAL METHOD

We build upon and employ the open-source software Basilisk C [1, 2] to simulate the draining bubbly sheet. The utilized code is shared openly in our repository [3]. The governing equations are solved using the one-fluid approximation [4], with surface tension incorporated as singular body force at the liquid-gas interface [5]. To account for the gas phase, we maintain a constant Ohnesorge number based on air viscosity, i.e., $Oh_a = 2 \times 10^{-5}$, and a constant density ratio $\rho_g/\rho = 0.001$. The liquid-gas interface is tracked using the Coupled Level Set volume of fluid (CLSVoF) method. CLSVoF combines some of the advantages of VoF and Level Set (LS) method [1, 6, 7]; this method is mass conserving, which is the advantage of VoF, while the curvature is estimated using the signed distance function, which is the advantage of LS. The interface is tracked using the VoF method governed by the advection equation

$$\frac{\partial \Psi}{\partial t} + \boldsymbol{\nabla} \cdot (\Psi \boldsymbol{u}) = 0. \tag{3}$$

where Ψ represents the VoF color function. We implement a geometric VoF approach reconstructing the interface at each time step, while the signed distance field d is advected as a tracer, which is obtained from VoF reconstruction of the interface. The distance is combined with the existing distance using a small weight. Finally, d is used to estimate the surface tension forces acting as singular forces [5, 8]. The explicit treatment of surface tension imposes a time step constraint based on the smallest capillary wave oscillation period [8].

The axisymmetric liquid sheet is simulated in the computational domain spanning $6R_0 \times 6R_0$. A bubble is placed centered on the axis and off the distance χ from the center of the sheet. At the domain boundaries, velocity conditions are imposed, i.e., $u = \omega (6R_0)$ and $v = -2\omega (6R_0)$, while the pressure gradients are set to zero for both liquid and gas phases. The domain is discretized using quadtree grids with adaptive mesh refinement (AMR) [8]. Error tolerances for the VoF color function, curvature, and velocity are set to 10^{-3}, 10^{-6}, and 10^{-3}, respectively.

III. CHARACTERIZE AND ESTIMATE THE INITIAL CAVITY SHAPE INFLUENCED BY ADDITIONAL PHYSICAL INHOMOGENEITIES

As discussed in the main text, in realistic scenarios, chemical or thermal inhomogeneities can delay initial hole nucleation. This delay leads to the formation of a wider thin film region near the poles, which eventually bursts to create a larger cavity. To simulate the initial shape of the sheet with a cavity, we conduct simulations where the interfaces of the bubble and sheet do not coalesce. When the sheet interfaces come into contact with bubble interfaces, instead of merging to create the cavity, sheet interfaces persist on bubble interfaces without coalescence. This is accomplished numerically by introducing different tracers for bubble and surrounding air. The time evolution for non-coalescing simulations is shown in fig. 1. At any time t_r, the thin bridge region is manually ruptured to obtain the cavities characterized by θ – large t_r corresponds to wider cavities, and thus, large θ. Therefore, for simulations to assess the effect of different initial cavities, the initial condition is taken as the profile at time t_r after removing the thin film cap. This approach has been widely adopted in numerous studies related to floating bubbles [9, 10].

The initial cavity profile is characterized by the angle $\theta(Bo, t_r)$, which is obtained by selecting the parameters Bo, and t_r. However, remarkably, the shape is observed to be the same, regardless of Bo, and t_r as long as $\sqrt{Bo} \times t_r$ is same. Thus, the initial cavity shape $\theta(\sqrt{Bo}\, t_r)$ is observed to be solely determined by $\sqrt{Bo} \times t_r$ for $Bo < 10^{-2}$ which includes almost all the realistic scenarios. For higher $Bo > 10^{-2}$, unlike small Bo cases, the minimum bubble-sheet thickness is no longer at the poles; instead, a small liquid volume is sandwiched at the poles, and the minimum thickness is observed off the poles. This observation poses a resemblance with the drop impact phenomenon [11], where for small Stokes number St, no air bubble is entrapped below the droplet. Also, the minimum thickness of the drop-plate interface is at the poles–similar behavior is observed here for $Bo < 10^{-2}$. In contrast, for larger St, air bubbles are entrapped, and the minimum thickness is observed away from the poles, which is similar to behavior here at larger $Bo > 10^{-2}$.

IV. EFFECTS OF BUBBLE ASYMMETRY χ/R_0

When the bubbles are placed asymmetrically in axial direction ($\chi/R_0 > 0$), the sheet no longer ruptures immediately, and the presence of the intact liquid bridge reduces the tendency of the sheet to break compared to the corresponding symmetric case, which is the least stable one. In the asymmetric cases illustrated in fig. 2, the darker zones depict the regions where the effect of the initial bubble on bubble breakup is still prominent. These regions are narrower
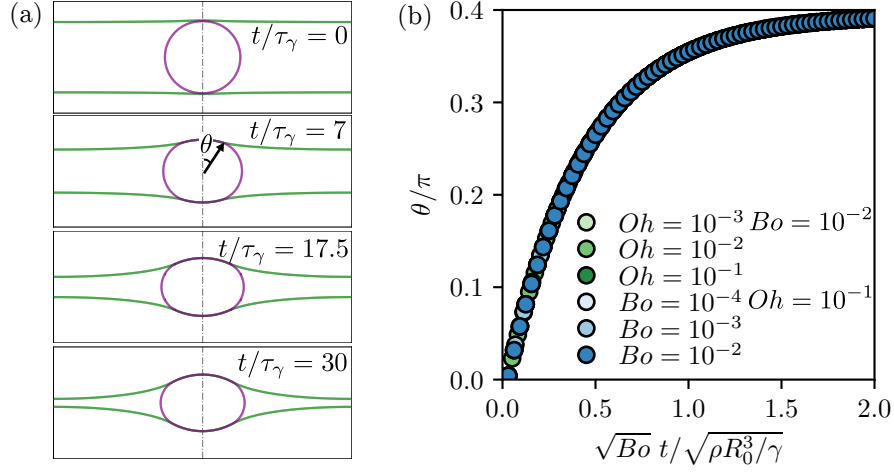
FIG. 1. (a) The time evolution of the draining sheet when the bubble-sheet interfaces do not coalesce at $Oh = 0.1$, and $Bo = 10^{-3}$. The green and magenta depict the sheet and bubble interfaces, respectively. The shape is characterized by the angle θ, which is the circumferential angle covered by the overlapping bubble-sheet interfaces. (b) The evolution of θ against $\sqrt{Bo}\, t_r/\sqrt{\rho R_0^3/\gamma}$ for various Bo and Oh higlights that the shape evolves independently of Bo and Oh and is solely determined by $\sqrt{Bo}\, t_r/\sqrt{\rho R_0^3/\gamma}$.

compared to the opening regime of symmetric cases at the right side of the gray transition line, bolstering the fact that the addition of asymmetricity reduces the tendency of sheets to break. As χ/R_0 increases, the effect of the asymmetry becomes even more pronounced. That is, the tendency of the sheets to break reduces even further. This aspect is also evident in fig. 2 where the lighter yellow regions enlarge, while the darker zones shrink as one increases χ/R_0 from 0.05 to 0.15.
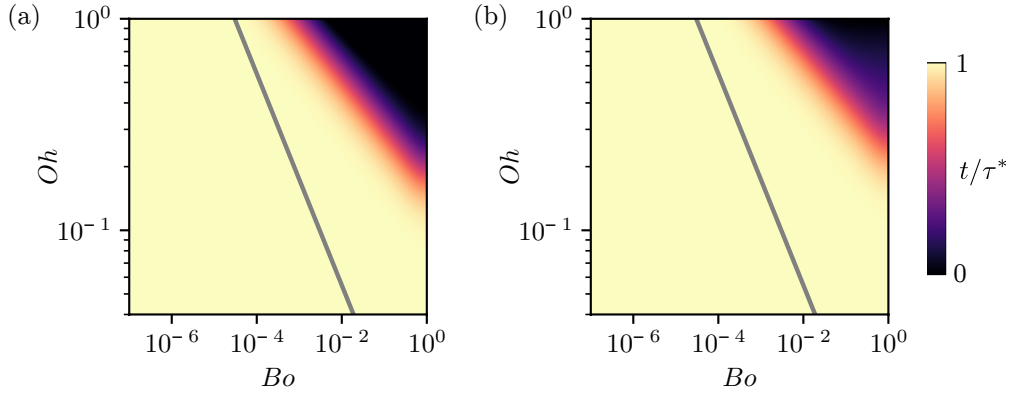

FIG. 2. Sheet breakup time (normalized by the no-bubble case rupture time $\tau^* \sim \tau_\gamma/\sqrt{Bo}$) in the $Oh - Bo$ parameter space, at (a) $\chi/R_0 = 0.05$, and (b) $\chi/R_0 = 0.15$. The gray line depicts the transition observed for symmetric cases ($\chi/R_0 = 0$).

[1] S. Popinet and collaborators, Basilisk C, http://basilisk.fr (Last accessed: April, 2025), 2013–2025.
[2] S. Popinet, *A quadtree-adaptive multigrid solver for the Serre–Green–Naghdi equations*, J. Comput. Phys. **302**, 336 (2015).
[3] A. K. Dixit and V. Sanjay, Code repository: Holey Sheets, https://github.com/comphy-lab/HoleySheet, 2025.
[4] G. Tryggvason, R. Scardovelli, and S. Zaleski, *Direct Numerical Simulations of Gas–Liquid Multiphase Flows* (Cambridge University Press, ADDRESS, 2011).
[5] J. U. Brackbill, D. B. Kothe, and C. Zemach, *A continuum method for modeling surface tension*, J. Comput. Phys. **100**, 335 (1992).
[6] M. Sussman and E. G. Puckett, *A coupled level set and volume-of-fluid method for computing 3D and axisymmetric incompressible two-phase flows*, J. Comput. Phys. **162**, 301 (2000).

[7] M. Saini, V. Sanjay, Y. Saade, D. Lohse, and S. Popinet, *Implementation of integral surface tension formulations in a volume of fluid framework and their applications to Marangoni flows*, arXiv preprint arXiv:2502.02712 (2025).

[8] S. Popinet, *An accurate adaptive solver for surface-tension-driven interfacial flows*, J. Comput. Phys. **228**, 5838 (2009).

[9] L. Duchemin, S. Popinet, C. Josserand, and S. Zaleski, *Jet formation in bubbles bursting at a free surface*, Phys. Fluids **14**, 3000 (2002).

[10] L. Deike, E. Ghabache, G. Liger-Belair, A. K. Das, S. Zaleski, S. Popinet, and T. Séon, *Dynamics of jets produced by bursting bubbles*, Phys. Rev. Fluids **3**, 013603 (2018).

[11] W. Bouwhuis, R. C. A. van der Veen, T. Tran, D. L. Keij, K. G. Winkels, I. R. Peters, D. van der Meer, C. Sun, J. H. Snoeijer, and D. Lohse, *Maximal air bubble entrainment at liquid-drop impact*, Phys. Rev. Lett. **109**, 264501 (2012).